IEEE Photonics Journal
An IEEE Photonics Society Publication

Large Bandwidth Photonic Microwave Image Rejection Mixer With High Conversion Efficiency

Volume 9, Number 3, June 2017

Wu Zhang
Aijun Wen, *Senior Member, IEEE*
Yongsheng Gao
Shuo Shang
Hanxiao Zheng
Hongye He

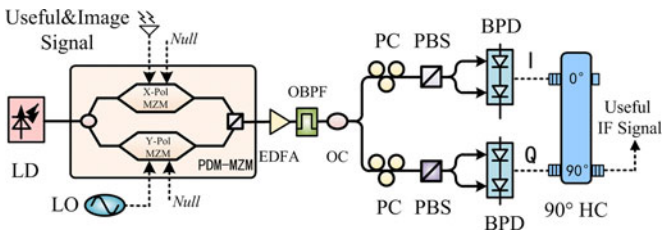

DOI: 10.1109/JPHOT.2017.2681663
1943-0655 © 2017 IEEE

Large Bandwidth Photonic Microwave Image Rejection Mixer With High Conversion Efficiency

Wu Zhang,[1] Aijun Wen,[1] *Senior Member, IEEE*, Yongsheng Gao,[2] Shuo Shang,[1] Hanxiao Zheng,[1] and Hongye He[1]

[1]State Key Laboratory of Integrated Service Networks, Collaborative Innovation Center of Information Sensing and Understanding, Xidian University, Xi'an 710071, China
[2]School of Electronics and Information, Northwestern Polytechnical University, Xi'an 710072, China

DOI:10.1109/JPHOT.2017.2681663

Manuscript received January 21, 2017; revised March 7, 2017; accepted March 9, 2017. Date of publication March 13, 2017; date of current version May 1, 2017. This work was supported in part by the National Natural Science Foundation of China under Grant 61306061 and in part by the China 111 Project (B08038). Corresponding author: A. Wen (e-mail: ajwen@xidian.edu.cn).

Abstract: A photonic microwave image rejection mixer (IRM) with large operating frequency range and high conversion efficiency is presented in this paper. The scheme is achieved by using a photonic microwave phase shifter, which is based on a polarization-division multiplexing Mach–Zehnder modulator (PDM-MZM). Thanks to the large operating frequency range of the photonic microwave phase shifter, the operating frequency of the proposed IRM can extend to 40 GHz. Besides, the system has high conversion efficiency, owing to the suppression of the optical carrier and application of balanced photodetector. To verify the scheme, an experiment is performed. Experimental results demonstrated large operating frequency range (5–40 GHz) and high image rejection ratio (40 dB) of the mixer. Compared with the conventional photonic microwave mixer, a 19-dB improvement of conversion efficiency is realized in the experiment.

Index Terms: Image rejection mixer (IRM), Polarization-division multiplexing Mach–Zehnder modulator (PDM-MZM), photonic microwave phase shifter, high conversion efficiency.

1. Introduction

The mixer is an essential component of defense receiver systems [1]. However, there are lots of inevitable image signals in electronic warfare environment. Because down-converted image signals have the same frequency with the useful IF signal, they may cause false reception. The mixer with image rejection ability can be used to solve the problem. Nevertheless, the limited bandwidth of conventional electrical image rejection mixers cannot meet the high bandwidth requirement of next generation electronic warfare system. Many researchers are trying to find solutions in the field of the microwave photonics [2], [3] for its advantages of high bandwidth, immunity to electromagnetic interference (EMI), as well as its light weight and small size [4], [5].

Many schemes based on microwave photonics to implement image rejection mixer have been proposed in the past few years. Most of them are based on phase cancellation method [6], which was reported by Hartley in 1992. The bandwidth of the original method is narrow for the use of directly modulated laser diode. A photonic microwave image rejection mixer (IRM) aimed to expand the bandwidth is proposed in [7]. It replaces narrow-bandwidth direct modulation with wideband

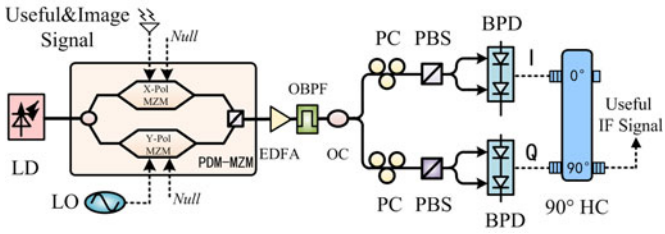

Fig. 1. Schematic diagram of the photonic microwave IRM. LD, laser diode; PDM-MZM, polarization-division multiplexing Mach–Zehnder modulator; LO, local oscillator; EDFA, erbium doped fiber amplifier; OBPF, optical band-pass filter; OC, 3-dB optical coupler; PC, polarization controller; PBS, polarization beam splitter; BPD, balanced photo-detector; 90° HC, electrical low-frequency 90° hybrid coupler.

external modulation. However, the scheme utilized a paralleled structure which contains two Mach–Zehnder modulators (MZM) and two photo-detectors (PD), and the paralleled structure leads to a complicated and bulky system. A photonic microwave IRM based on an integrated dual-parallel Mach–Zehnder modulator (DPMZM) is presented in [8], but the scheme includes a large-bandwidth 90° hybrid coupler (HC) which has the problem of amplitude and phase imbalance at different operating frequency. A photonic microwave IRM based on a dual-polarization dual-drive Mach-Zehnder (DPol-DMZM) modulator is presented in [9]. However, this IRM needs large-bandwidth power splitters to split the radio frequency (RF) signal and local oscillator (LO) signal equally before they are applied to the modulator. The large-bandwidth power splitter also has the frequency-dependency problem. Apart from the phase cancellation method, some straight-forward methods which use filters to filter out the image signals before they are down-converted are reported in [10], [11], these methods are always complex and not suitable for wideband system.

A photonic microwave IRM based on a wideband photonic phase shifter is proposed in this paper. The wideband photonic microwave phase shifter is used to obtain the quadrature IF signals. Then by combing the quadrature IF signals through an electrical low-frequency 90° HC, the image signal can be suppressed while the useful signal is strengthened. Since no large-bandwidth 90° HC and power splitter are used in the system, the operating frequency range of the mixer is large. In addition, the mixer has high conversion efficiency for the suppression of the optical carrier and the use of balanced photo-detector (BPD). Because of the advantages of wideband and high conversion efficiency, the system is desirable for future wideband receiver systems.

2. Principles

Fig. 1 is the system schematic diagram of the proposed photonic microwave IRM. It consists of a laser diode (LD), a polarization-division multiplexing Mach–Zehnder modulator (PDM-MZM), an erbium doped fiber amplifier (EDFA), an optical band-pass filter (OBPF), a 3-dB optical coupler (OC), and two pairs of polarization controllers (PC), polarization beam splitters (PBS), balanced photo-detectors (BPD), as well as an electrical low-frequency 90° hybrid coupler (HC). The optical carrier from the LD is injected into the PDM-MZM. The PDM-MZM is composed of an optical coupler, X-Pol and Y-Pol sub-modulator and a polarization beam combiner (PBC), as depicted in Fig. 1. In our scheme, the X-Pol and Y-Pol sub-modulator of the PDM-MZM are single driven by RF signal and LO signal respectively, and they both work at null point to implement double sideband suppressed carrier modulation (DSB-SC). The optical sidebands after the sub-modulators are polarization multiplexed by the PBC, and the polarization multiplexing signal is amplified by the following EDFA. The OBPF is used to select upper sidebands of the polarization multiplexing signal. The selected optical sidebands are sent to an OC which is used to divide the optical signals into I path and Q path equally. In each path, a PC, a PBS and a BPD are used to construct the rest of the photonic microwave phase shifter, and the phase of the IF signal after the BPD can be tuned easily by controlling the PC. Finally, the 90° HC is used to combine the IF signals which output from the BPDs.

The optical carrier from the LD can be expressed as $E_{in}(t) = E_o \exp j(\omega_c t)$, E_o and ω_c are its amplitude and angular frequency. The LO signal with angular frequency of ω_{LO} and amplitude of V_{LO} can be written as $V_{LO}\sin(\omega_{LO} t)$. Similarly, the useful signal and image signal can be expressed as $V_U \sin(\omega_U t)$ and $V_{IM}\sin(\omega_{IM} t)$, respectively.

In this scheme, the null biased X-Pol sub-modulator is driven by useful signal and image signal. If the insertion loss of the modulator is ignored, the signal outputs from the X-Pol sub-modulator can be expressed as

$$E_X(t) = \frac{E_{in}(t)}{\sqrt{2}} \cdot \begin{Bmatrix} J_1(\beta_U)\left[\exp(j\omega_U t) - \exp(-j\omega_U t)\right] \\ +J_1(\beta_{IM})\left[\exp(j\omega_{IM} t) - \exp(-j\omega_{IM} t)\right] \end{Bmatrix} \tag{1}$$

where $\beta_u = (V_u/V_\pi)\cdot\pi$, $\beta_{IM} = (V_{IM}/V_\pi)\cdot\pi$ are the modulation indexes of the useful signal and image signal, and V_π represents the half-wave voltage of the X-Pol sub-modulator.

In the same way, the signal output from the Y-Pol sub-modulator is expressed as

$$E_Y(t) = \frac{E_{in}(t)}{\sqrt{2}} \cdot \{J_1(\beta_{LO})\left[\exp(j\omega_{LO} t) - \exp(-j\omega_{LO} t)\right]\} \tag{2}$$

The upper sidebands of the polarization multiplexing signal are selected by the OBPF. It can be given as

$$\begin{aligned} E_{OBPF}(t) &= \begin{bmatrix} E_x(t), \\ E_Y(t) \end{bmatrix} \\ &= \frac{E_{in}(t)}{2} \cdot \begin{bmatrix} J_1(\beta_U)\exp(j\omega_U t) \\ +J_1(\beta_{IM})\exp(j\omega_{IM} t), \\ J_1(\beta_{LO})\exp(j\omega_{LO} t) \end{bmatrix} \end{aligned} \tag{3}$$

To explain the principle of the photonic microwave phase shifter, the transformation matrix of the PC and PBS is given by

$$T_{PC-PBS} = \begin{bmatrix} \cos\theta & -\sin\theta\cdot\exp(j\varphi) \\ \sin\theta\cdot\exp(j\varphi) & \cos\theta \end{bmatrix} \tag{4}$$

where θ is the angle between the principle state of the light and the principle axis of the PBS, and φ is the phase difference between the X and Y polarization state induced by the PC.

In I path, the signal after the PBS can be expressed as

$$\begin{aligned} E_{PBS-I}(t) &= \left[E_{PBS-I1}(t), E_{PBS-I2}(t)\right] \\ &= \left[E_x(t), E_y(t)\right] T_{PC} \\ &= \frac{E_{in}(t)}{2\sqrt{2}} \begin{bmatrix} J_1(\beta_U)\exp(j\omega_U t) + J_1(\beta_{IM})\exp(j\omega_{IM} t), \\ J_1(\beta_{LO})\exp(j\omega_{LO} t) \end{bmatrix} \\ &\quad \cdot \begin{bmatrix} \cos\theta & -\sin\theta\cdot\exp(j\varphi) \\ \sin\theta\cdot\exp(j\varphi) & \cos\theta \end{bmatrix} \\ &= \frac{E_{in}(t)}{2\sqrt{2}} \begin{bmatrix} J_1(\beta_U)\exp(j\omega_U t)\cos\theta \\ +J_1(\beta_{IM})\exp(j\omega_{IM} t)\cos\theta \\ +J_1(\beta_{LO})\exp(j\omega_{LO} t)\sin\theta\exp(j\varphi), \\ -J_1(\beta_U)\exp(j\omega_U t)\sin\theta\exp(j\varphi) \\ -J_1(\beta_{IM})\exp(j\omega_{IM} t)\sin\theta\exp(j\varphi) \\ +J_1(\beta_{LO})\exp(j\omega_{LO} t)\cos\theta \end{bmatrix} \end{aligned} \tag{5}$$

where $E_{PBS-I1}(t)$, $E_{PBS-I2}(t)$ represent the upper and lower output signals of the PBS of I path.

Then the θ is set at 45° by adjusting PC, (5) can be rewritten as

$$E_{PBS-I}(t) = \frac{E_{in}(t)}{4}\begin{bmatrix} J_1(\beta_U)\exp(j\omega_U t) \\ +J_1(\beta_{IM})\exp(j\omega_{IM} t) \\ +J_1(\beta_{LO})\exp(j\omega_{LO} t)\exp(j\varphi), \\ -J_1(\beta_U)\exp(j\omega_U t)\exp(j\varphi) \\ -J_1(\beta_{IM})\exp(j\omega_{IM} t)\exp(j\varphi) \\ +J_1(\beta_{LO})\exp(j\omega_{LO} t) \end{bmatrix}. \tag{6}$$

The optical signal is injected into the BPD. After balanced photo-detection, the IF signals can be expressed as

$$\begin{aligned} i_{BPD-I}(t) &= \eta\left[E_{PBS-I1}(t)\cdot E^*_{PBS-I1}(t) - E_{PBS-I2}(t)\cdot E^*_{PBS-I2}(t)\right] \\ &\propto \frac{\eta}{4}\begin{bmatrix} J_1(\beta_U)J_1(\beta_{LO})\cos((\omega_U-\omega_{LO})t-\varphi) \\ +J_1(\beta_{IM})J_1(\beta_{LO})\cos((\omega_{LO}-\omega_{IM})t+\varphi) \end{bmatrix} \end{aligned} \tag{7}$$

where η denotes the responsivity of the BPD

As seen from (7), the phase (φ) of the IF signal can be tuned easily by adjusting the PC. Quadrature IF signals are desired to achieve the photonic microwave IRM, the quadrature IF signals in I path and Q path are given by

$$i_{BPD-I}(t) \approx \frac{\eta}{4}\begin{bmatrix} J_1(\beta_U)J_1(\beta_{LO})\cos((\omega_U-\omega_{LO})t) \\ +J_1(\beta_{LO})J_1(\beta_{IM})\cos((\omega_{LO}-\omega_{IM})t) \end{bmatrix} \tag{8}$$

$$i_{BPD-Q}(t) \approx \frac{\eta}{4}\begin{bmatrix} J_1(\beta_U)J_1(\beta_{LO})\sin((\omega_U-\omega_{LO})t) \\ -J_1(\beta_{LO})J_1(\beta_{IM})\sin((\omega_{LO}-\omega_{IM})t) \end{bmatrix}. \tag{9}$$

Then an electrical low-frequency 90° HC is used to combine the quadrature IF signals. The output of the 90° HC is expressed as

$$\begin{aligned} i_u(t) &= \frac{\eta}{4}\begin{bmatrix} J_1(\beta_U)J_1(\beta_{LO})\cos((\omega_U-\omega_{LO})t) \\ +J_1(\beta_{LO})J_1(\beta_{IM})\cos((\omega_{LO}-\omega_{IM})t) \\ +J_1(\beta_U)J_1(\beta_{LO})\sin((\omega_U-\omega_{LO})t+\pi/2) \\ -J_1(\beta_{LO})J_1(\beta_{IM})\sin((\omega_{LO}-\omega_{IM})t+\pi/2) \end{bmatrix} \\ &= \frac{\eta}{2}J_1(\beta_U)J_1(\beta_{LO})\cos((\omega_U-\omega_{LO})t). \end{aligned} \tag{10}$$

As can be seen from (10), the down-converted image signal is suppressed while the down-converted useful signal is strengthen. The optical carrier is suppressed in this scheme, and the optical power is not occupied by the optical carrier which does not carry useful information anymore. Furthermore, the optical power in the other polarization is also sent to BPD for photo-detection. In other words, there is a 3-dB improvement of the optical power before the photo-detection. It is well known that the 3-dB improvement of the optical power will lead to an improvement of 6 dB in conversion efficiency. Therefore, the mixer has higher conversion efficiency.

3. Experiment and Results

An experiment based on the structure depicted in Fig. 1 is conducted to verify the scheme. A LD (Emcore1782) is used to generate the optical carrier with the wavelength of 1552 nm and the power of 17 dBm. The PDM-MZM (Fujitsu FTM7980) whose half-wave voltage of each sub-modulator is about 7 V is cascaded with the LD. The 40-GHz useful signal (or 39-GHz image signal) with power of 5 dBm is supplied by a signal source (R&S SMBV100A), and another signal source (Agilent 83630B) is used to generate a 39.5-GHz LO signal with the power of 11 dBm.

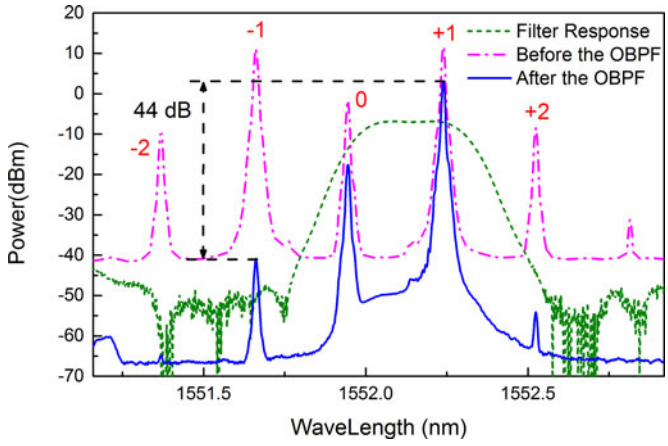

Fig. 2. Optical spectra of the polarization multiplexing signal when measured before the OBPF (dash dot line) and after the OBPF (solid line). Dash line represents the response of the OBPF.

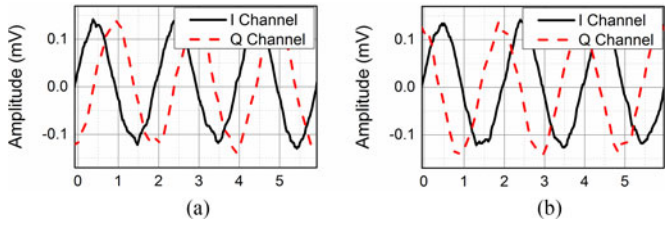

Fig. 3. Waveforms of the IF signals when −90 (a) and 90 (b) phase shift between IF signals in I and Q path are conducted. (a) Time (ns). (b) Time (ns).

For the compensation of the insert loss of the modulator (7 dB), an erbium doped fiber amplifier (EDFA) which works at automatic power control (APC) mode with 17 dBm output power is placed between the modulator and the OBPF. The OBPF is followed by the 3-dB OC. In each path of the 3-dB OC, the PC, PBS and BPD are cascaded in series. The responsivity of the BPD is 0.7 A/W. After the BPDs, a low-frequency electrical 90° HC (Hirose HDH00803) with operating frequency of 0.5–1 GHz is used to combine the IF signals. During the experiment, an optical spectrum analyzer (YOKOGAWA AQ6370C) with resolution of 0.01 nm is used to measure the optical spectra, and a spectrum analyzer (R&S FSW50) and an oscilloscope (TK DSO) are adopted to measure the electrical spectra and waveforms of the IF signals.

In our scheme, the RF signal and LO signal are both DSB-SC modulated, and the upper sidebands of modulated signal are selected by the OBPF. The optical spectra of the signals before (dash dot line) and after (solid line) the OBPF are given in Fig. 2. In addition, the filter response (dash line) is also shown in Fig. 2. Although making distinction between the sidebands of RF signal and LO signal is difficult owing to the limited resolution (0.01 nm), the 44-dB suppression ratio of the -1st-order sidebands relative to +1st-order sidebands can be seen from Fig. 2. Thanks to the high out-band rejection ratio of the OBPF, the optical signal after the OBPF will be mainly occupied by the +1st-order sidebands of LO signal and RF signal.

As theoretically demonstrated in the principle, the LD, PDM-MZM, PC, PBS can compose a photonic microwave phase shifter. In order to show the phase shift ability of the photonic microwave phase shifter, the measured waveforms of IF signals with and without phase shift are shown in Fig. 3. As seen from Fig. 3, a relative −90° (see Fig. 3(a)) and 90° (see Fig. 3(b)) phase shift between the IF signals in I and Q path are conducted successfully. The waveforms are distorted due to the low sampling rate of our oscilloscope.

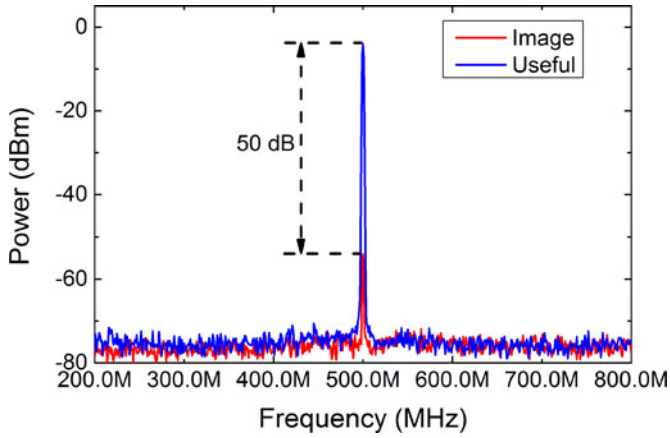

Fig. 4. Electrical spectra of the down-converted useful signal and image signal.

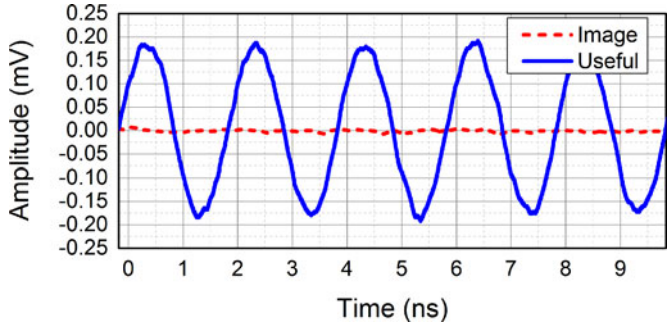

Fig. 5. Waveforms of the down-converted useful signal and image signal.

In our experiment, the frequency of the useful signal and the image signal is 40 GHz and 39.5 GHz respectively, and the LO signal frequency is 39.5 GHz. Thus, the down-converted useful signal and down-converted image signal have the same frequency of 500 MHz (500 MHz = 40 GHz – 39.5 GHz = 39.5 GHz – 39 GHz). If the mixer works well, the 500-MHz down-converted image signal should be suppressed while the 500-MHz useful IF signal should not be damaged. Fig. 4 shows the electrical spectra of the down-converted useful signal and image signal. As seen from Fig. 4, the power of the 500-MHz useful IF signal is high and the suppression ratio (IRR) of the image signal can reach 50 dB. To show the image rejection ability intuitively, the waveforms of the down-converted useful signal and image signal are given in Fig. 5. The peak-to-peak value of the down-converted image signal is nearly zero while the down-converted useful signal has good amplitude.

The conversion efficiency of the system is high not only owing to the elimination of the optical carrier but the use of the BPD as well. In our scheme, the power of the RF signal is set at 5 dBm, and the power of received IF signal is -4.1 dBm; thus the conversion efficiency can be calculated as -9.1 dB. It is much higher than traditional mixer's conversion efficiency (~ -28 dB typically) [12]. The conversion efficiency for different RF frequency is given in Fig. 6(a). The conversion efficiency is low under 10 GHz owing to the filter influence of the OBPF. The comparison of the power of the received IF signal with single PD and with BPD is also made during the experiment and the experimental result is given in Fig. 6(b). The power improvement of 5.85 dB agrees well with theory.

To demonstrate the large operating bandwidth of the scheme, the IRRs for different RF signal frequency are measured. As seen from Fig. 7(a), the IRRs for different frequencies are all above 40 dB. It verifies the large operating bandwidth of our scheme. Furthermore, the 40-dB IRR is higher than the IRRs of electrical IRMs ($\sim$30 dB typically). In order to verify the performance of the

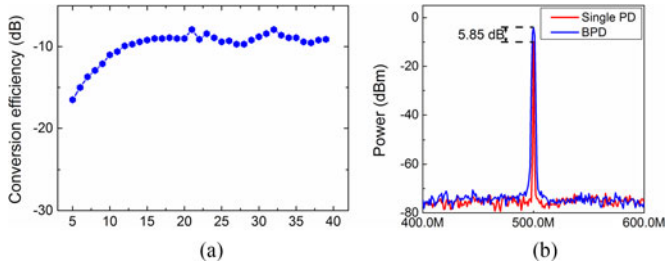

Fig. 6. Relationship of the conversion efficiency with the different RF frequency (a) and the comparison of the IF signal with Sing PD and BPD (b). RF (GHz). Frequency (MHz).

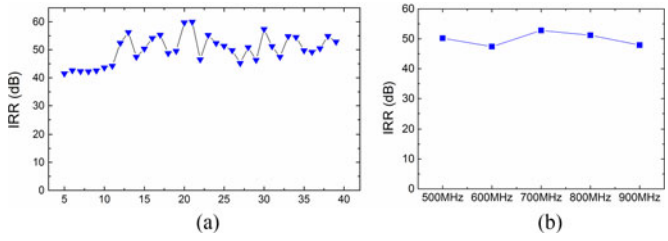

Fig. 7. Relationship of the IRR with different frequency of RF (a) and IF (b).

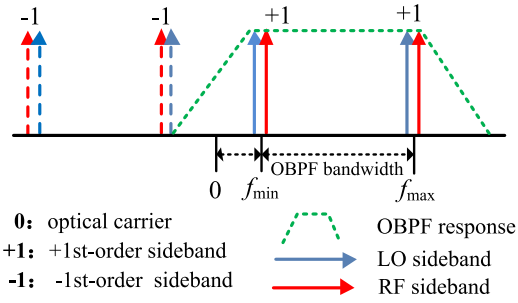

Fig. 8. OBPF influences the operating frequency range of the system.

low-frequency 90° HC, the IRR with different IF signal frequency is given in Fig. 7(b). The stability of the low-frequency 90° HC can be guaranteed by the result shown in Fig. 7(b).

The OBPF affects the operating frequency range. As shown in Fig. 8, the minimum operating frequency (f_{min}) of the scheme is determined by the slope of the OBPF. The OBPF should filter out the negative-order optical sidebands when selects the positive-order optical sidebands. The maximum operating frequency of the proposed approach ($f_{max} = f_{min} +$ bandwidth) is restricted by the bandwidth (>50 GHz) of the OBPF.

The photonic microwave IRM can work in higher frequency, but it cannot be demonstrated due to limited frequency (0–40 GHz) of the signal sources. In practical application, like other methods based on external modulation, bias drifting problem cannot be avoided in this scheme. However, there are commercially available bias controllers to solve this problem.

4. Conclusion

In this paper, a photonic microwave image rejection mixer with large operating bandwidth is proposed. No large-bandwidth 90° HC and power splitter are used, and only a low-frequency electrical 90° HC is included in this scheme. Therefore, its bandwidth is not limited by conventional electrical

components. Experimental results show that the IRR can reach more than 40 dB when the frequency of RF signal ranges from 5 GHz to 40 GHz. The mixer also has high conversion efficiency thanks to the carrier suppression and the use of BPD.

References

[1] A. C. Lindsay, G. A. Knight, and S. T. Winnall, "Photonic mixers for wide bandwidth RF receiver applications," *IEEE Trans. Microw. Theory Techn.*, vol. 43, no. 9, pp. 2311–2317, Sep. 1995.

[2] J. Capmany, B. Ortega, D. Pastor, and S. Sales, "Discrete-time optical processing of microwave signals," *J. Lightw. Technol.*, vol. 23, no. 2, pp. 702–723, Feb. 2005.

[3] J. Capmany and D. Novak, "Microwave photonics combines two worlds," *Nature Photon.*, vol. 1, no. 6, pp. 319–330, Jun. 2007.

[4] J. Yao, "Microwave photonics," *J. Lightw. Technol.*, vol. 27, no.3, pp. 314–335, Feb. 2009.

[5] V. J. Urick *et al.*, "Long-haul analog photonics," *J. Lightw. Technol.*, vol. 29, no. 8, pp. 1182–1205, Apr. 2011.

[6] H. Ogawa and H. Kamitsuna, "Fiber optic microwave links using balanced laser harmonic generation, and balanced/image cancellation laser mixing," *IEEE Trans. Microw. Theory Techn.*, vol. 40, no. 12, pp. 2278–2284, Dec. 1992.

[7] L. Chao, C. Wenyue, and J. F. Shiang, "Photonic mixers and image-rejection mixers for optical SCM systems," *IEEE Trans. Microw. Theory Techn.*, vol. 45, no. 8, pp. 1478–1480, Aug. 1997.

[8] J. Zhang, E. H. W. Chan, X. Wang, X. Feng, and B. Guan, "High conversion efficiency photonic microwave mixer with image rejection capability," *IEEE Photon. J.*, vol. 8, no. 4, Aug. 2016, Art. no. 3900411.

[9] Z. Tang and S. Pan, "Image-reject mixer with large suppression of mixing spurs based on a photonic microwave phase shifter," *J. Lightw. Technol.*, vol. 34, no. 20, pp. 4729–4735, Oct. 2015.

[10] S. J. Strutz and K. J. Williams, "A 0.8-8.8-GHz image rejection microwave photonic downconverter," *IEEE Photon. Technol. Lett.*, vol. 12, no. 10, pp. 1376–1378, Oct. 2000.

[11] S. J. Strutz and K. J. Williams, "An 8-18-GHz all-optical microwave downconverter with channelization," *IEEE Trans. Microw. Theory Techn.*, vol. 49, no. 10, pp. 1992–1995, Oct. 2001.

[12] E. H. W. Chan and R. A. Minasian, "Microwave photonic downconverter with high conversion efficiency," *J. Lightw. Technol.*, vol. 30, no. 23, pp. 3580–3585, May 2012.